Continental sources, transoceanic transport, and interhemispheric exchange of carbon monoxide over the Pacific

JOURNAL OF GEOPHYSICAL RESEARCH, VOL. 106, NO. D23, PAGES 32,571–32,589, DECEMBER 16, 2001

Continental sources, transoceanic transport, and interhemispheric exchange of carbon monoxide over the Pacific

A.C. Staudt, D. J. Jacob, and J. A. Logan

Department of Earth and Planetary Sciences and Division of Engineering and Applied Sciences Harvard University Cambridge, Massachusetts

D. Bachiochi and T. N. Krishnamurti

Department of Meteorology, Florida State University, Tallahassee, Florida

G. W. Sachse

NASA Langley Research Center, Hampton, Virginia

Abstract.

The Pacific Exploratory Mission to the Tropics phase B (PEM-Tropics B) aircraft campaign in March-April 1999 surveyed the chemical composition of the Pacific atmosphere from 35°N to 35°S and up to 12 km altitude. We use these observations in combination with a global three-dimensional model driven by assimilated meteorological observations to investigate the transport of northern hemispheric pollutants over the Pacific. We focus on carbon monoxide (CO) and tag it in the model by its region of origin. The model reproduces the observed large-scale latitudinal, longitudinal, and vertical gradients of CO concentrations over the Pacific. Biomass burning in Southeast Asia, which was particularly intense in spring 1999, contributed most of the CO enhancements observed in the free troposphere over the northern tropical Pacific but played only a minor role in the boundary layer. Fossil fuel combustion in Europe and Asia contributed most of the observed CO enhancements in the boundary layer over the North Pacific; the European influence dominated over Asian influence north of 35°N. European influence over the Pacific is particularly strong in spring because of wintertime accumulation of CO at high latitudes. North American pollution made little contribution to CO anywhere over the Pacific. Circulation of Eurasian industrial pollution around the Pacific High and into the trade winds produced a tropical "river of pollution" flowing in the lower troposphere from the northeastern to the western equatorial Pacific and in the vicinity of the South Pacific Convergence Zone. This pathway, however, made little contribution to interhemispheric exchange. Elevated concentrations observed for CO and other northern hemispheric tracers in the upper troposphere over the southeastern Pacific provide evidence for efficient interhemispheric exchange through a narrow region of upper tropospheric westerlies in the eastern equatorial Pacific (the "westerly duct"). We find that this westerly duct was the most important pathway for global interhemispheric exchange during PEM-Tropics B. It was particularly well developed because of the La Nina conditions.

1. Introduction

Better understanding and quantification of the contributions from different source regions to global atmospheric pollution is a major theme in tropospheric chemistry research with implications for climate change [*Mickley et al.*, 1999], the oxidizing power of the atmosphere [*Thompson*, 1992], and surface air quality [*Jacob et al.*, 1999; *Jaffe et al.*, 1999]. The Pacific Exploratory Mission to the Tropics phase B (PEM-Tropics B), a NASA Global Tropospheric Experiment (GTE) aircraft campaign conducted over the tropical Pacific in March-April 1999 [*Raper et al.*, this issue], provided excellent data for examining long-range transport of pollution over a particularly remote region of the world. The campaign employed two aircraft, a DC-8 and a P-3B, oper-

Paper number 2001JD900078.
0148-0227/01/2001JD900078$09.00

ating out of California, Hawaii, Christmas Island, Fiji, Tahiti, and Easter Island. Flights during PEM-Tropics B extensively surveyed the Pacific from 40°S to 40°N with numerous vertical profiles. The PEM-Tropics B observations complement those obtained during previous GTE campaigns over the Pacific, namely, PEM-Tropics A [*Hoell et al.*, 1999], which surveyed a similar domain during August-September 1996, and PEM-West A and B [*Hoell et al.*, 1996, 1997], which characterized outflow from Asia over the northwest Pacific during August-September 1991 and February-March 1994, respectively.

In this study, we examine the long-range transport and continental signatures of combustion effluents over the North and South Pacific by interpreting the PEM-Tropics B aircraft observations with a global three-dimensional (3-D) chemical transport model (CTM) driven by assimilated meteorological observations. Our analysis focuses on a simulation of carbon monoxide (CO), a product of both fossil fuel combustion and biomass burning. Carbon monoxide is removed from the atmosphere mainly by oxidation by the hydroxyl radical (OH). The atmospheric lifetime of CO ranges from about a month in the tropics to over a year at high latitudes in winter, long enough to allow significant intercontinental and interhemispheric transport yet short enough to maintain high variability in the distribution.

The atmosphere over the North Pacific is expected to be heavily impacted by circumpolar westerly transport of pollutants emitted from the northern midlatitudes continents (Europe, North America, and Asia). Over the Pacific this westerly flow curves southward and subsides around the subtropical Pacific High, delivering pollutants to the tropics [*Merrill*, 1989]. Chemical signature analyses of the PEM-Tropics B observations north of 10°N indicate that air masses sampled in the marine boundary layer were strongly influenced by urban and industrial sources, whereas those in the midtroposphere were strongly influenced by biomass burning [*Logan et al.*, 2000; *Blake et al.*, this issue]. These results are consistent with back trajectories computed by *Fuelberg et al.* [this issue] for surface air over the northeastern tropical Pacific, which frequently originate from high latitudes over the Eurasian continent before being drawn around the Pacific High. The back trajectories corresponding to biomass burning pollution in the midtroposphere generally originate over Southeast Asia, where biomass burning was at its seasonal maximum. Back trajectories, however, have only limited capability for source region identification because of the long transport times over the Pacific and over the continents upwind. Analysis with a global 3-D model, as presented here, offers better insights.

The chemical signatures observed over the northeastern Pacific during PEM-Tropics B are consistent with those observed over the northwest Pacific in the same season during PEM-West B. *Blake et al.* [1997] found that air masses sampled north of 25°N and below 6 km during PEM-West B had strong urban and industrial influences, while those sampled south of 25°N had strong biomass burning influences. A global 3-D model analysis of the PEM-West B Asian outflow by I. *Bey et al.* (Asian outflow to the Pacific Ocean in springtime: Origins, pathways, and budgets, submitted to *Journal of Geophysical Research*, 2001b, hereinafter referred to as *Bey et al.*, submitted manuscript, 2001b) identified frontal lifting into the lower free troposphere followed by rapid transport in the westerlies as the dominant export mechanism from eastern Asia. Whereas air masses with an urban origin were exported mainly in the boundary layer and lower free troposphere, those influenced by biomass burning were more often exported in the middle and upper troposphere.

Transport of northern midlatitudes pollutants to the tropics and into the southern troposphere is critical in terms of their ultimate implications for global atmospheric chemistry and climate change. PEM-Tropics B took place during a strong El Nino-Southern Oscillation (ENSO) cold phase, often referred to as La Nina conditions. The Intertropical Convergence Zone (ITCZ), a barrier for cross-equatorial flow in the lower troposphere, was less defined than on average over the Pacific during PEM-Tropics B both because of normal seasonal variability and because convection is weaker in the central Pacific during La Nina conditions [*Fuelberg et al.*, this issue]. Another major barrier to horizontal transport over the Pacific is the South Pacific Convergence Zone (SPCZ) which extends along a southeast-northwest axis across the South Pacific and merges with the ITCZ at its northern end. La Nina conditions during PEM-Tropics B caused the SPCZ to be shifted westward of its typical position [*Fuelberg et al.*, this issue], creating a window in the vicinity of the dateline where northern hemispheric air could travel into the southern hemisphere near the surface, as we will show later. Past studies have associated La Nina conditions with enhanced interhemispheric exchange because of the shifts in the ITCZ and the SPCZ [*Halter et al.*, 1988; *Merrill*, 1989; *Prinn et al.*, 1992; *Hartley and Black*, 1995; *Harris and Oltmans*, 1997].

La Nina conditions can also foster enhanced interhemispheric transport in the upper troposphere. The westward movement of maximum sea surface temperatures is associated with a northwesterly mean flow in the eastern equatorial Pacific upper troposphere [*Newell et al.*, 1996]. During PEM-Tropics B this northwesterly flow was associated with a clockwise circulation centered over Christmas Island (2°N, 155°W) [*Fuelberg et al.*, this issue], similar to observations for previous La Nina conditions [*Arkin*, 1982]. Past studies have found that this northwesterly flow in the eastern Pacific upper troposphere is associated with elevated perturbation kinetic energy and enhanced propagation of Rossby waves into the southern hemisphere [*Arkin and Webster*, 1985; *Tomas and Webster*, 1994]. We will use the PEM-Tropics B observations over the southern tropi-

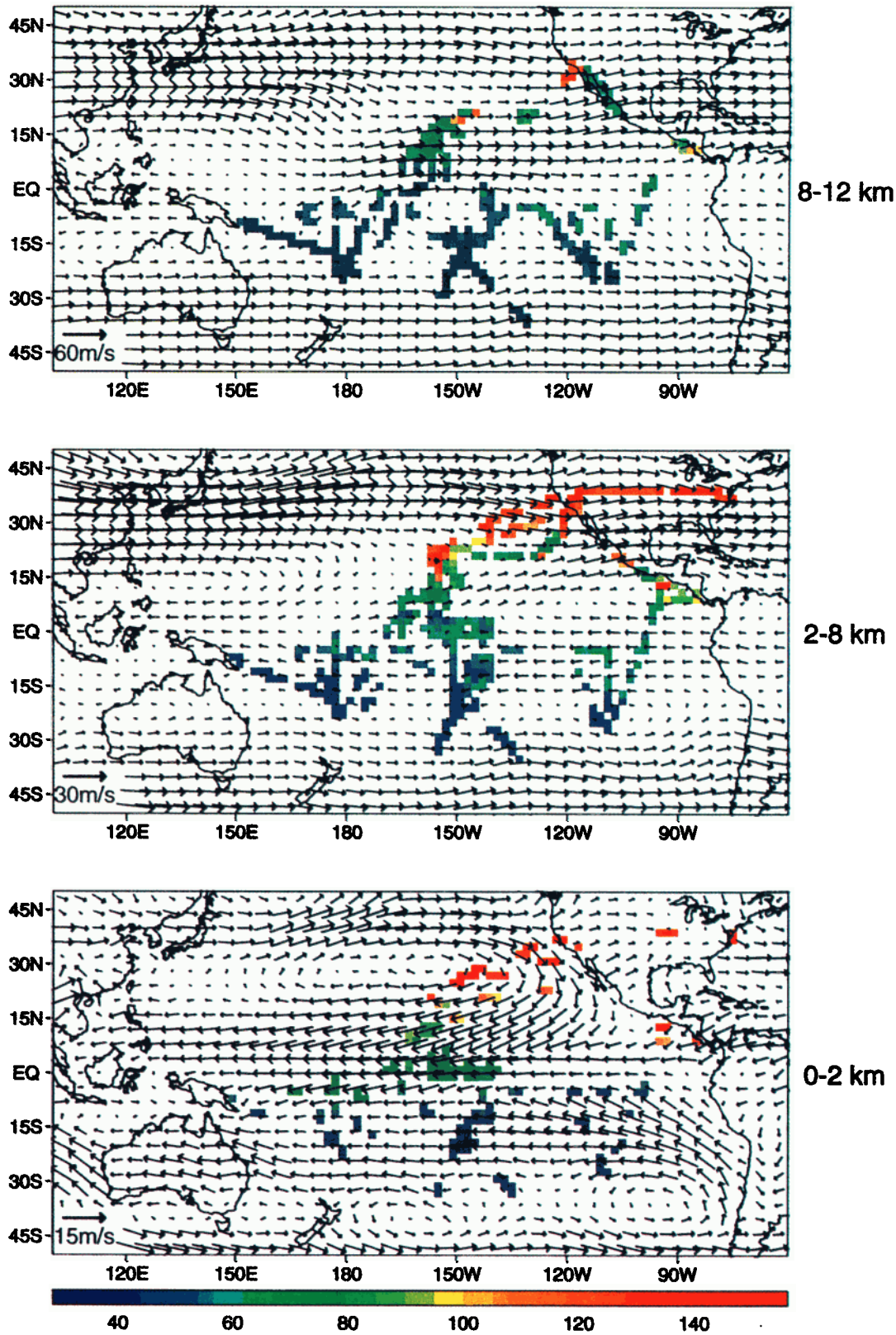

Plate 1. Observed CO concentrations (in ppb) during PEM-Tropics B averaged into 2.5° latitude by 2.5° longitude bins for three altitude ranges (0–2 km, 2–8 km, 8–12 km). Superimposed are mean horizontal wind vectors for the PEM-Tropics B time period (March 1 to April 19, 1999) for representative altitudes in each range (1000 hPa, 500 hPa, 200 hPa). Winds are from the FSU reanalysis. The arrow length is proportional to the wind speed.

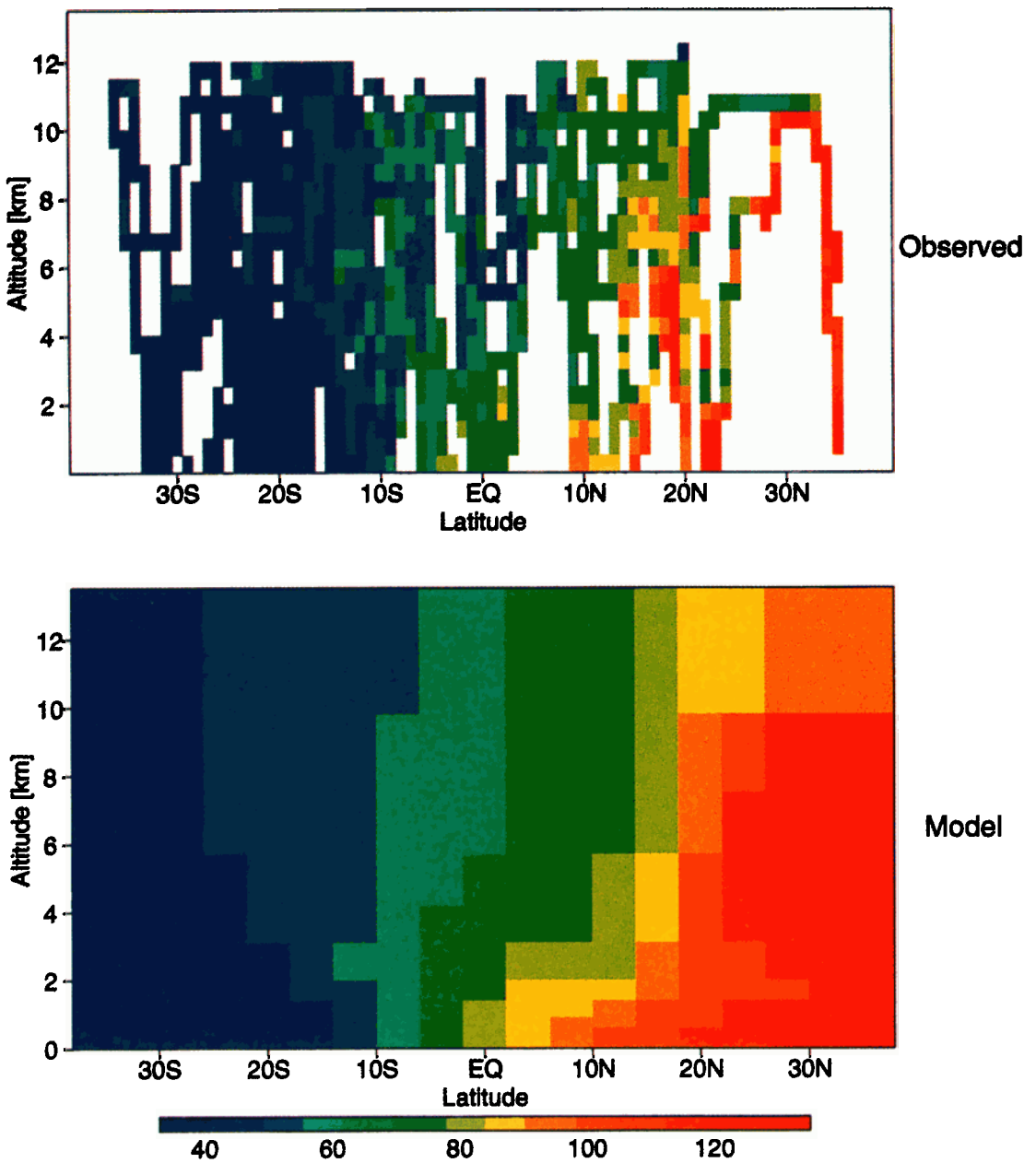

Plate 2. Carbon monoxide concentrations (in ppb) over the tropical Pacific during PEM-Tropics B (March 1 to April 19, 1999). (top) Observations averaged in 1° latitude by 0.5 km altitude bins over all longitudes covered in PEM-Tropics B (see Plate 1). (bottom) Results from the Harvard/FSU CTM for the same time period and averaged over the same domain as the observations.

cal Pacific to show that the same propagation mechanism applies to chemical tracers, and we will assess the corresponding contribution to global interhemispheric exchange.

2. Observed CO Distribution During PEM-Tropics B

Carbon monoxide was measured at 1 Hz resolution on both aircraft during PEM-Tropics B with a differential absorption technique using a tunable diode laser in the 4.7-μm CO band [*Sachse et al.*, 1987, 1991; *Pougatchev et al.*, 1999]. The measurements were conducted for a total of 275 hours over the Pacific between the DC-8 aircraft (0–12 km altitude range) and the P-3B aircraft (0–7 km). Flight tracks during PEM-Tropics B included extensive vertical profiling from the boundary layer to the ceilings of both aircraft, resulting in broad spatial coverage.

Maps of the composite CO concentrations measured from both aircraft are shown in Plate 1 for three altitude ranges. These CO observations are averaged across longitudes in Plate 2a to show the variation with altitude and latitude (the model distribution in Plate 2b will be discussed in section 3). A north-south concentration gradient is evident at all altitudes, but is much steeper in the lower than in the upper troposphere. Concentrations decrease with altitude in the northern hemisphere but increase weakly with altitude in the southern hemisphere south of 10°S, for reasons that will be examined in section 3.

Concentrations of CO over the South Pacific are much lower and show considerably less variability than during PEM-Tropics A, when a strong biomass burning influence was evident [*Schultz et al.*, 1999]. Mean concentrations of CO over the South Pacific (10–30°S, 0–12 km) were 66 ± 17 ppbv in PEM-Tropics A and 46 ± 6 ppbv in PEM-Tropics B. PEM-Tropics B was conducted in the wet season of the austral tropics, when biomass burning influence in the southern hemisphere is minimum.

The longitudinal concentration gradients of CO observed in PEM-Tropics B are much weaker than the latitudinal gradients because of the stronger zonal flow. Nevertheless, the CO data over the South Pacific show significant large-scale gradients of increasing concentrations from east to west in the lower troposphere, and increasing concentrations from west to east in the upper troposphere (Plate 2). These gradients are related to processes of interhemispheric exchange, as will be discussed in sections 5 and 6.

Concentrations measured in the northern hemisphere during PEM-Tropics B are more variable than in the southern hemisphere. High concentrations of CO were observed in the midtroposphere of the northeastern Pacific (Plate 1). *Blake et al.* [this issue] associate this enhancement with biomass burning outflow from Southeast Asia on the basis of correlations with CH_3Cl, a biomass burning tracer. Biomass burning in Southeast Asia is at a seasonal maximum during March-April and was particularly extensive in India during 1999 (B. N. Duncan, personal communication, 2001). Elevated CO concentrations were also observed in the lower troposphere (0–2 km) on flights between California and Hawaii (Plate 1). This air had a distinct urban and industrial signature [*Blake et al.*, this issue]. The enhancement of CO in the lower troposphere extends into the western equatorial Pacific as far south as 10°S due to transport by the northern trade winds, forming a "river of pollution," as illustrated in the bottom panel of Plate 1. This river of pollution produces a wedge of northern hemispheric air extending into the southern hemisphere, as seen in the mean latitudinal gradient (Plate 2) up to 2–3 km altitude. Other tracers predominantly produced by urban and industrial activities in the northern hemisphere, including C_2H_6, C_2H_2, HCFC-141b, H-1211, and C_2Cl_4, exhibited spatial patterns in the boundary layer similar to CO during PEM-Tropics B [*Blake et al.*, this issue].

3. Model Description and Evaluation

The Harvard/Florida State University (FSU) CTM provides a global simulation of tropospheric O_3-NO_x-CO-hydrocarbon chemistry during the PEM-Tropics B period. It is driven by assimilated meteorological fields produced by the FSU Global Spectral Model [*Krishnamurti et al.*, 1993, 1996] for January 22 to April 19, 1999. A detailed treatment of tropical dynamics makes the FSU analysis especially useful for studies of the tropical Pacific. In particular, the precipitation rates used in the physical initialization process are derived from satellite observations of outgoing longwave radiation and precipitation [*Krishnamurti et al.*, 1983; *Gairola and Krishnamurti*, 1992]. The CTM has a horizontal resolution of 4° latitude by 5° longitude, and 14 vertical layers along a sigma coordinate centered at 0.99, 0.95, 0.9, 0.85, 0.8, 0.7, 0.6, 0.5, 0.4, 0.3, 0.2, 0.1, 0.07, 0.03; the corresponding vertical resolution is about 0.5 km in the lower troposphere and 1–3 km in the middle and upper troposphere.

Transport processes in the CTM include grid-scale advection using a second-order moments scheme [*Prather*, 1986], dry convection which mixes tracer uniformly from the surface up to the mixed layer height calculated by the FSU model, and deep moist convection which is parameterized as a subgrid process using upward convective mass fluxes computed in the FSU model. Starting at the bottom of each convective column, the amount of air that must be moved upwards out of the box by deep moist convection is entrained into a "pipe" and carried upward to the next grid box. If the upward convective mass flux through the top of this next grid box is greater than the flux through the bottom, then the air already in the convective pipe is preserved, and additional air is entrained into the pipe to reflect the convective mass flux convergence; the air in the pipe is

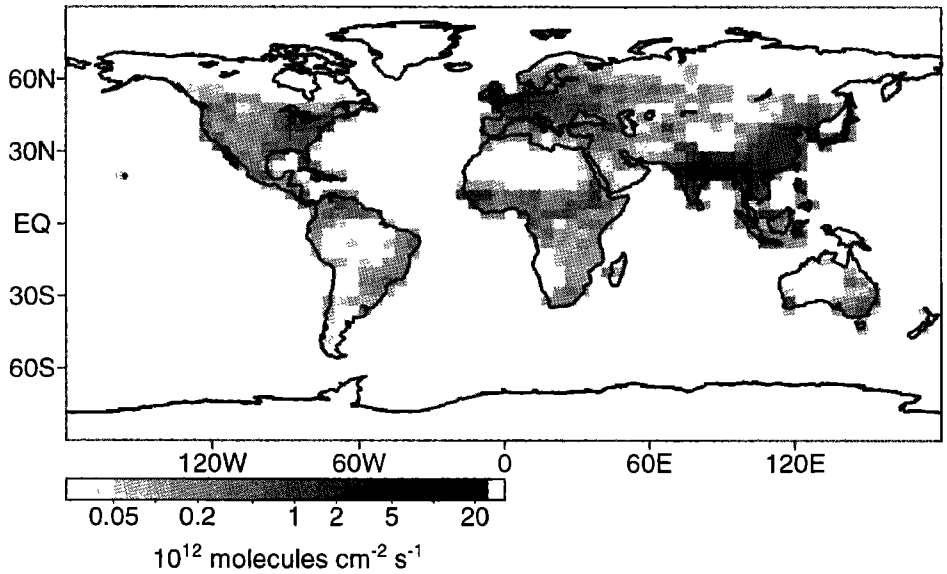

Figure 1. Emissions of CO from fossil fuel, biofuel, and biomass combustion sources during PEM-Tropics B (March 1 to April 19, 1999).

transported upward to the next grid box, and the process is repeated. When the pipe encounters a grid box where the convective mass flux through the top is less than through the bottom, then it is partially or totally detrained into that grid box. Compensatory large-scale subsidence outside the pipe allows the grid column to retain its original air mass distribution, so that convection results in no net transport of air mass.

The CTM transports 24 tracers to represent tropospheric O_3-NO_x-CO-hydrocarbon chemistry. The chemical mechanism is that of *Horowitz et al.* [1998] with minor updates as discussed by I. *Bey et al.* (Global modeling of tropospheric chemistry with assimilated meteorology: Model description and evaluation, submitted to *Journal of Geophysical Research*, 2001a, hereinafter referred to as *Bey et al.*, submitted manuscript, 2001a) and it is integrated in the CTM with a fast Gear solver [*Jacobson and Turco*, 1994]. The Fast-J radiative transfer code of *Wild et al.* [2000], including Mie scattering by clouds, is used to compute photolysis rates (vertically distributed cloud optical depths are taken from the FSU meteorological fields). Wet and dry deposition are as described by *Bey et al.* (submitted manuscript, 2001a). Emissions of CO, NO_x, and hydrocarbons from fossil fuel combustion and industry are implemented as described by *Wang et al.* [1998a] for 1985. They are scaled to 1995 levels, the most recent year for which data could be obtained, as described by *Bey et al.* (submitted manuscript, 2001a). For this scaling, national inventories for countries with air pollution control regulations are used when available [*Environmental Protection Agency (EPA)*, 1997; *European Monitoring and Evaluation Programme (EMEP)*, 1997]. For other countries, CO and hydrocarbon emissions are scaled to trends in liquid fuel CO_2 emissions, and NO_x emissions are scaled to trends in total CO_2 emissions from fossil fuel combustion [*Marland et al.*, 1999]. Biofuel emissions in the *Wang et al.* [1998a] inventory have been updated following the work of R. M. Yevich and J. A. Logan (personal communication, 2000). Nitrogen oxide emissions from lightning are parameterized following *Pickering et al.* [1998] and *Price and Rind* [1992] and are adjusted to yield a global source of 6 Tg N yr^{-1}, within the accepted range of 1–20 Tg N yr^{-1} [*Huntrieser et al.*, 1998]. Biogenic emissions of NO_x and organic species are as described by *Wang et al.* [1998a] with minor modifications (*Bey et al.*, submitted manuscript, 2001a).

Biomass burning emissions for the PEM-Tropics B period are specified using fire count observations from the Along Track Scanning Radiometer-2 (ATSR-2) satellite. These fire counts are applied as scaling factors to a climatological inventory of biomass burning emissions for CO and other gases from R. M. Yevich and J. A. Logan (personal communication, 2000). The scaling is done using a 20-year record of satellite fire observations from Total Ozone Mapping Spectrometer (TOMS) [*Hsu et al.*, 1996] and ATSR-2 to define a fire climatology (B. N. Duncan, personal communication, 2001). We apply emission factors (g of species emitted/kg C burned), mostly following the recommendations of *Andreae and Merlet* [2001]. During March-April, biomass burning takes place in the Indian subcontinent, Southeast Asia, Indonesia, northern Africa, Central America, and northern South America. Biomass burning emissions from the Indian subcontinent and Southeast Asia were 30% larger than the 20-year average during 1999, mostly due to intense burning in India where there were 5 times as many fire counts during 1999 than during either of the previous 2 years of observations. Burning in Central America was 40% less than average, while burning in other regions was close to average. The distribu-

Table 1. Global Distribution of CO Emissions During PEM-Tropics B (March 1 to April 19, 1999)[a]

	Fossil Fuel	Biofuel	Biomass Burning
North America (180°–25°W, 0°-90°N)	13.6	1.1	4.9
Europe/North Africa (25°W-70°E, 0°–90°N)	15.5	4.9	10.3
Asia (70°E-180°, 0°–90°N)	17.0	11.8	62.5
South America (180°–25°W, 0°–90°S)	1.5	2.1	0.7
Southern Africa (25°W–70°E, 0°–90°S)	0.6	1.6	1.2
Indonesia and Australia (70°E–180°, 0°–90°S)	1.2	0.8	4.4
Total	49.3	22.3	84.1

[a]Units are in teragrams.

tion of anthropogenic CO emissions in the model from fossil fuel, biofuel, and biomass combustion is shown in Figure 1 for the PEM-Tropics B period and regional emission totals for these different sources are summarized in Table 1. The anthropogenic CO emissions fall within the range estimated by other global models [*Holloway et al.*, 2000; *Bey et al.*, submitted manuscript, 2001a].

Simulations are conducted for a 3-month period from January 22 to April 19, 1999. The model is initialized on January 21 with mean January concentrations from the full-year CTM simulation of *Wang et al.* [1998a] using general circulation model meteorology. These initial conditions provide a good approximation to observed climatological CO [*Wang et al.*, 1998b]. Simulation through March 1 provides initialization of the transport patterns in the model, and we focus our attention on the March 1 to April 19 period.

Results from the full chemistry simulation will be described in detail in a future paper. The simulated March-April distribution of OH concentrations is comparable to that obtained by other models and consistent with the known lifetime of methylchloroform [*Spivakovsky et al.*, 2000]. The resulting average lifetime for CO (Figure 2) is 63 days and shows considerable latitudinal variation, in a manner similar to that obtained by other global models [*Holloway et al.*, 2000; *Bey et al.*, submitted manuscripts, 2001b]. The minimum lifetime is 30 days at 20°N, reflecting high OH concentrations caused by a combination of clear skies and high water vapor [*Spivakovsky et al.*, 2000]. North of 50°N the lifetime in March-April is in excess of 6 months, so that loss of CO is actually controlled by transport to lower latitudes.

The model reproduces the general features of the observed CO distribution above the tropical Pacific, as illustrated in Plate 2b. The vertical resolution, although relatively coarse, is sufficient to resolve the large-scale vertical gradients. The wedge of higher CO concentrations in the lower troposphere extending into the southern hemisphere, associated with the river of pollution (section 2), is well simulated. Concentrations decrease with altitude in the northern hemisphere due to surface sources. In the southern hemisphere, CO increases slightly with altitude due to faster cross-equatorial transport in the upper troposphere. This reversal of the vertical gradient between the northern and the southern hemisphere has been previously obtained in CTMs for tracers of northern hemispheric origin [*Prather et al.*, 1987; *Jacob et al.*, 1987; *Kanakidou et al.*, 1991, 1995]. Although an increase of CO with altitude has been observed in aircraft sampling near Cape Grim, Australia [*Pak et al.*, 1996], PEM-Tropics B provides the first experimental verification of this vertical gradient reversal in the tropics through extensive observations from 30°S–30°N during a period free of large biomass burning contamination.

A more detailed evaluation of the simulated CO is shown in Figure 3 by the latitudinal concentration gradients in different altitude ranges from 0 to 12 km. The

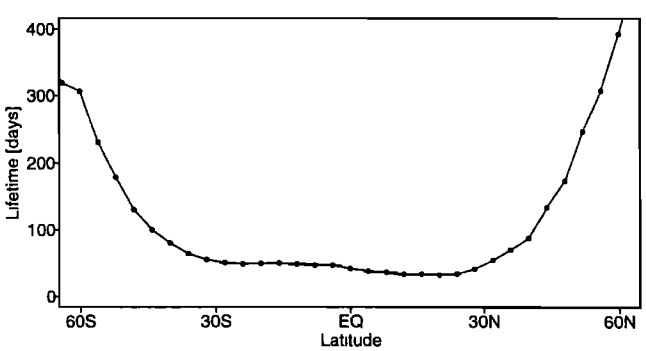

Figure 2. Atmospheric lifetime of CO versus latitude during PEM-Tropics B (March 1 to April 19, 1999). Values are zonal averages for the tropospheric column.

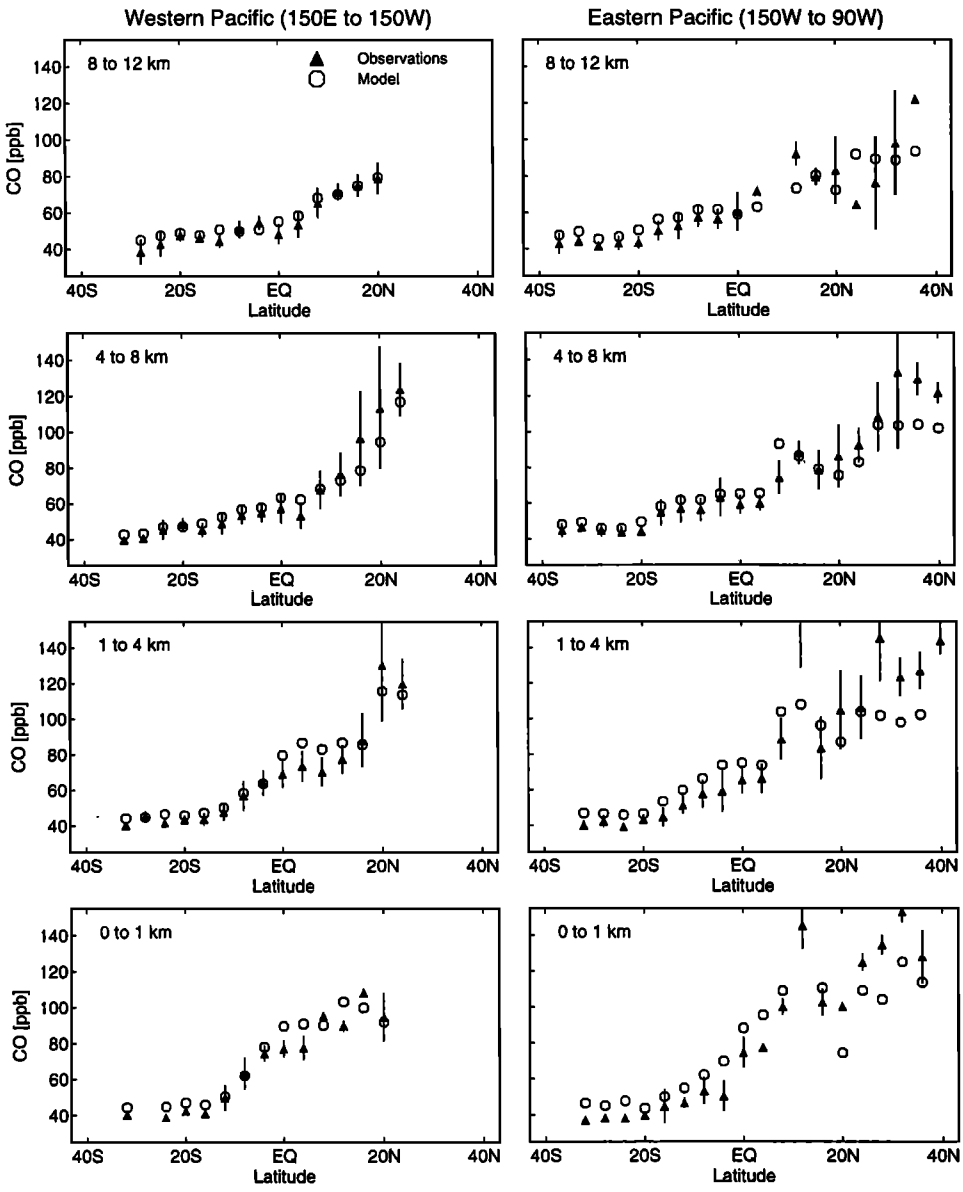

Figure 3. Latitudinal gradients of observed and modeled CO concentrations over the western and eastern Pacific in four altitude ranges from 0 to 12 km. The PEM-Tropics B observations (solid triangles) are averaged over March 1 to April 19, 1999, the altitude and longitude ranges specified in the figure, and 4° latitude bins. Vertical bars indicate standard deviations. The model (open circles) is sampled along the flight tracks and for the flight days, and the results are averaged across the same longitude and altitude ranges as the observations.

model here is sampled along the flight tracks and for the specific flight days. The western and eastern Pacific are separated; there are no observations in the western Pacific north of 20°N. The major model flaws are a 5 ppbv overestimate over the South Pacific, a 10–20 ppb overestimate at 0°–10°N over the western Pacific, and a 10–20 ppb overestimate at 15°S–10°N in the eastern Pacific lower troposphere. Near the surface the ITCZ is an effective barrier to meridional transport, as illustrated by the steep concentration gradient between 10°S and 10°N in both the observations and the model. The observed boundary layer concentration of CO at 0°–10°S is about 20 ppbv higher in the western Pacific, where it is influenced by the river of pollution, as compared to the eastern Pacific. The model produces a similar but weaker longitudinal gradient. In the upper troposphere the north-south gradient is more gradual, and the longitudinal gradient is reversed both in the observations and in the model, for reasons that will be discussed in section 6. Observed and simulated concentrations of CO above 8 km at 0°–20°S are 5–10 ppb higher in the eastern Pacific than in the western Pacific.

Much of our analysis of source regions for polluted air masses over the Pacific will rely on a "tagged" CO simulation, in which CO is decomposed linearly into tracers representing different sources [*Granier et al.*, 2000; *Bey et al.*, submitted manuscript, 2001b]. We use a total of 20 tracers to resolve all 18 regional sources listed in

Table 1 plus chemical production from the oxidation of methane and isoprene. Isoprene emissions are converted to CO with a molar yield of 1.25 (A. Fusco, personal communication, 1999). Methane has an atmospheric concentration of 1.7 ppm and is converted to CO with a molar yield of 1. The source of CO from the oxidation of hydrocarbons other than methane and isoprene is neglected. Loss of the CO tracers is calculated using daily mean OH fields archived from the standard full chemistry simulation, so that the decomposition of CO into tagged tracers is fully linear. Concentrations of CO tracers are initialized on January 22 with output from a 2-year simulation using the GEOS-CHEM global 3-D model [*Bey et al.*, submitted manuscript, 2001a, 2001b]. The GEOS-CHEM model results for 1994 capture well the CO observations from PEM-Tropics B despite underestimating CO in other parts of the world. We verified that summing the concentrations of all tagged CO tracers reproduces the results from the standard full chemistry simulation to within the uncertainties introduced by ignoring the source of CO from nonmethane hydrocarbons, assuming a constant CO yield from isoprene, and using slightly different initial conditions.

4. Sources of CO Over the North Pacific

The distributions of column CO concentrations for four tagged tracers of continental emissions are shown in Plate 3. Fractional contributions from each source to the total CO in the northeastern tropical Pacific region (10°–35°N) sampled during PEM-Tropics B are given in Table 2. As expected, fuel emissions from Asia are a large component of the CO simulated over the North Pacific. Urban and industrial sources are mostly located in northeastern Asia (northern China, Korea, and Japan), where there is little convection during winter and early spring. Asian fuel CO is generally exported to the Pacific either directly in the boundary layer or in the lower free troposphere following lifting due to cold fronts passing over the Asian continent [*Yienger et al.*, 2000; *Bey et al.*, submitted manuscript, 2001b]. Once exported from Asia, CO travels across the Pacific in the prevailing midlatitude westerlies found at all altitudes.

The European contribution to fuel CO concentrations over the northeastern tropical Pacific is nearly as large as that from Asia, and it is larger at extratropical latitudes (Plate 3 and Table 2). During winter and early spring, long-range transport over the Eurasian continent is largely controlled by the Siberian High, which tends to confine surface emissions in the boundary layer and to carry air masses from Europe northward [*Raatz*, 1989]. Export from Europe has been shown to have a large impact on wintertime pollutant levels in the Arctic boundary layer [*Christensen*, 1997; *Novelli et al.*, 1998]. During winter, CO is chemically inert in the Arctic and can accumulate to high levels. It is eventually transported southward to the Pacific in the eastern branch of the Siberian High and from there around the Pacific High [*Raatz*, 1989; *Merrill*, 1989]. This transport mechanism enables European CO to have a large impact on the North Pacific atmosphere during spring, particularly in the boundary layer.

The North American contribution to CO over the northeastern tropical Pacific is only 7%, even though North America is the closest continent to the region. North American fuel emissions (including biofuels) are about 25% less than those from Europe and nearly 50% less than those from Asia (Table 1). The main export route for North American pollution is to the east. During winter and early spring, pollution exported over the Atlantic encounters the Bermuda High which tends to carry air southward to the eastern tropical Atlantic rather than to the Arctic. Some CO emitted in western and central North America is exported by the model northward and then incorporated into either the flow around the Aleutian Low located over the North Pacific or the flow around the Icelandic Low located over the North Atlantic. Only a small portion of North American CO is exported to the southwest where it enters the large-scale circulation around the Pacific High. The latter mechanism is known to cause major events of long-range transport of North American pollution to Hawaii in summer [*Galasyn et al.*, 1987; *Moxim*, 1990; *Balkanski et al.*, 1992], when the Pacific High is centered farther north. In spring the circulation around the Pacific High does not usually extend to the west coast of the United States (Plate 1).

The biomass burning contribution to CO columns in the northeastern Pacific domain sampled in PEM-Tropics B is comparable to the sum of all fuel sources (Table 2 and Plate 3). Almost all of this biomass burning contribution is from India and Southeast Asia, and it is far more important in the free troposphere than in the boundary layer (Table 2). The large contribution of biomass burning to free tropospheric CO is consistent with the 3-D model results of *Bey et al.* [submitted manuscript, 2001b], who found maximum biomass burning outflow from southeastern Asia to the Pacific in the subtropical free troposphere. As shown in Plate 3, the model simulates a local maximum of CO from biomass burning in the eastern subtropical Pacific. This local maximum occurs during April when the biomass burning source from Southeast Asia decreases substantially. The vestiges of the strong biomass burning emissions during March combined with increased stagnation northeast of Hawaii as the Pacific High migrates northward cause an accumulation of Asian biomass burning CO in the midtroposphere. Observations of elevated tracers of biomass burning in the middle troposphere of the northeastern tropical Pacific confirm a significant biomass burning influence in the region [*Logan et al.*, 2000; *Blake et al.*, this issue]. Biomass burning effluents in Central America and northern South America exported to the west in the trade winds have little effect on the northeastern Pacific but do influence the equatorial Pacific, as discussed below.

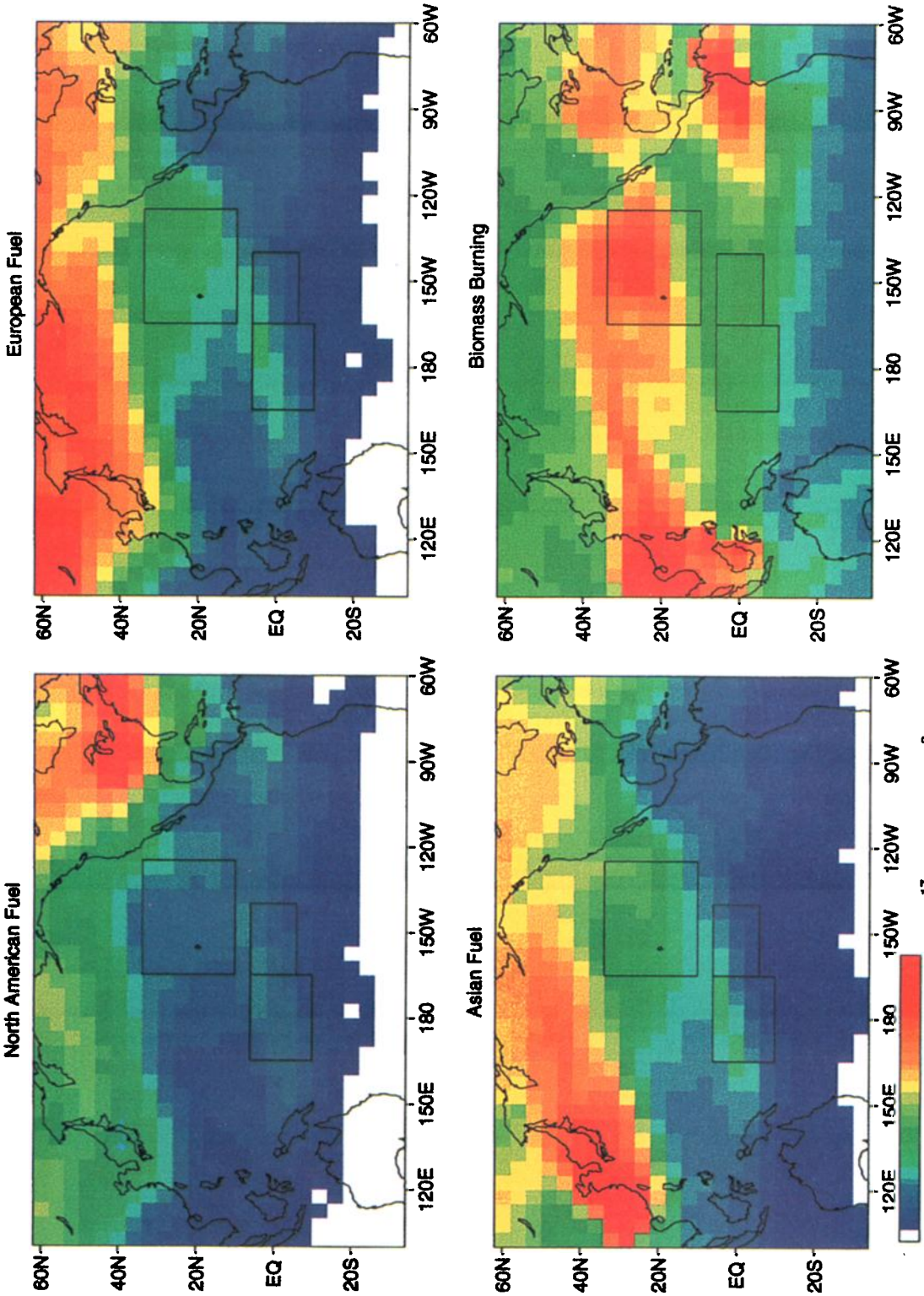

Plate 3. Simulated column CO (10^{17} molecules cm^{-2}) for four tagged CO tracers representing sources from total fuel consumption (fossil and biofuels) in North America, Europe, and Asia, and sources from biomass burning. The column concentrations are averaged over the PEM-Tropics B time period (March 1 to April 19, 1999). Rectangles identify regions used for further source analysis (Table 2).

Table 2. Source contributions to CO Concentrations Over the Pacific[a]

Source	Northeastern Tropical Pacific (10°–34°N, 165°–125°W) Tropospheric Column[b]	Northeastern Tropical Pacific 10°–34°N, 165°–125°W) Boundary Layer[c]	Central Equatorial Pacific (6°S–6°N, 165°–140°W) Boundary Layer[c]	Western Equatorial Pacific (10°S–6°N, 165°E–165°W) Boundary Layer[c]
Fuel combustion[d]				
North America	7	11	11	10
Europe	12	19	13	14
Asia	15	19	12	14
South hemisphere	1	1	1	1
Biomass burning				
Asia	20	11	6	7
Northern Africa	4	4	4	4
Central America	1	1	6	4
Other	2	1	2	2
Atmospheric production[e]				
North hemisphere	27	27	30	29
South hemisphere	11	6	15	15
Total	100	100	100	100

[a]Values are model averages for March 1 to April 19, 1999 as calculated from the linear decomposition of CO into tagged tracers with different sources (see text). Source contributions are in percent.
[b]The tropospheric column is defined as extending from 0 to 16 km altitude. Results are not sensitive to the specification of the top because stratospheric CO concentrations are low.
[c]The boundary layer is defined as extending from 0 to 2 km altitude.
[d]Including fossil fuels and biofuels.
[e]From oxidation of methane and isoprene. The CO source from oxidation of other hydrocarbons has been neglected in this analysis.

5. River of Pollution Across the Equatorial Pacific

We now turn our attention to analyzing the contributions from different source regions to the river of pollution observed in the lower troposphere across the equatorial Pacific during PEM-Tropics B (section 2). The modeled concentrations and fluxes of the four largest tagged CO tracers in near surface air (0.2–0.6 km altitude) are shown in Plate 4. The fuel tracers from the three northern hemispheric source continents are transported around the Pacific High and then travel southwestward from the California coast across the Pacific all the way to the SPCZ, which restricts further transport. We also see in Plate 4 that intrusion of northern hemispheric CO into the eastern equatorial Pacific is much weaker than in the west because of a better-defined ITCZ [*Fuelberg et al.*, this issue]. There is some export of CO to the eastern equatorial Pacific from biomass burning in Central America and northern South America. As discussed in section 3, biomass burning in Central America was lower than average in 1999.

Table 2 provides the fractional contribution of each CO source to the boundary layer for three segments of the river of pollution that were sampled during the campaign: the northeastern tropical Pacific, the central equatorial Pacific, and the western equatorial Pacific. These segments are identified by the rectangles in Plate 3. European and Asian fuel sources make comparable contributions to each subregion of the river of pollution. The North American fuel source makes a smaller contribution for reasons discussed in the previous section. Although biomass burning is a major component of the column CO in the North Pacific, we find that its contribution to the river of pollution is considerably smaller, consistent with the chemical signatures observed during PEM-Tropics B [*Logan et al.*, 2000, *Blake et al.*, this issue]. We attribute this result to the subtropical transport of biomass burning pollution in the free troposphere, followed by stagnation during subsidence in the Pacific High, which allows for extensive chemical destruction. The lifetime of CO at 25°–30°N, the principal axis for transport of biomass burning CO across the Pacific (Plate 3), is only 30 days (Figure 2). In contrast, Eurasian urban and industrial CO is transported at higher latitudes and in the lower troposphere, resulting in a longer lifetime and faster circulation around the Pacific High.

6. Interhemispheric Transport

Several mechanisms have been proposed to explain how air is exchanged between the hemispheres, includ-

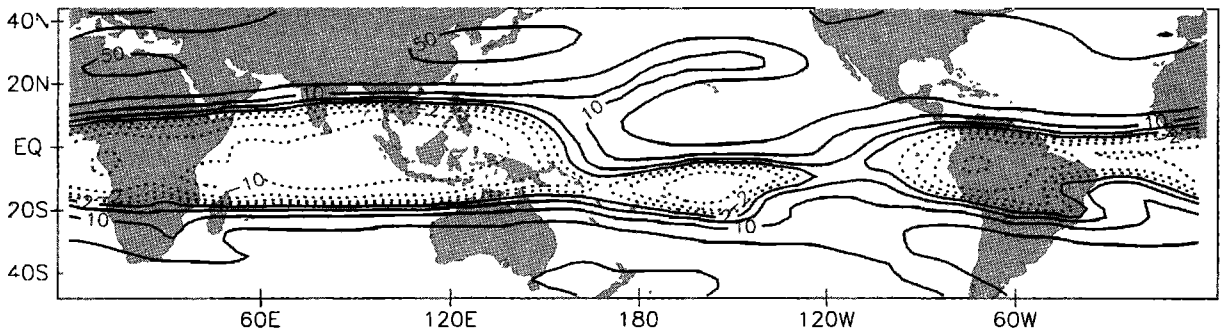

Figure 4. Zonal winds (m s^{-1}) at 200 hPa from the NCEP-NCAR reanalysis averaged for the PEM-Tropics B time period (March 1 to April 19, 1999). Positive values indicate westerly winds.

ing monsoonal flow, seasonal movements of the ITCZ causing the Hadley circulation cells to entrain air from the opposite hemisphere, and the ITCZ upper-level divergence associated with deep convection [*Kidson et al.*, 1969; *Newell et al.*, 1974, 1996; *Bowman and Cohen*, 1997]. Modeling studies have suggested that this last mechanism is the dominant pathway for cross-equatorial transport [*Prather et al.*, 1987; *Hartley and Black*, 1995]. However, few observations have been available in the tropical upper troposphere to confirm these model results.

Another mechanism that has been considered is cross-equatorial transport through regions of upper tropospheric equatorial westerlies termed "westerly ducts" [*Arkin and Webster*, 1985; *Prinn et al.*, 1992; *Tomas and Webster*, 1994; *Hartley and Black*, 1995]. Typically, cross-equatorial propagation of large-scale Rossby waves, which are associated with eddy activity and tracer transport (due to wave breaking), is inhibited by a band of easterlies. *Webster and Holton* [1982] identified regions of upper tropospheric equatorial westerlies, located above the eastern Pacific and Atlantic oceans, through which transient waves could propagate from mid-latitudes through the tropics into the other hemisphere. *Tomas and Webster* [1994] used potential vorticity along isentropic surfaces to show that this wave propagation does take place. During PEM-Tropics B, the westerly duct over the eastern Pacific was well developed (Figure 4) as is typically the case during boreal winter and during La Nina conditions [*Tomas and Webster*, 1994]. No duct was present over the eastern Atlantic at that time.

Prinn et al. [1992] suggested that transport of northern hemispheric air southward through the westerly duct over the Pacific could make a major contribution to interannual variability in measurements of methylchloroform at Samoa (14°S). Methylchloroform, which was produced predominantly in the northern hemisphere before being phased out in the 1990s [*Prinn et al.*, 1995], was higher at Samoa during La Nina conditions, indicating enhanced transport of northern hemispheric air into the southern tropics. However, general circulation model simulations of CFC-11 by *Hartley and Black* [1995] indicated that upper tropospheric divergence associated with deep convection, rather than flow through the westerly duct, was responsible for the majority of tracer transport to the southern hemisphere. They suggested that ENSO-driven shifts in the location of the SPCZ and ITCZ could explain the interannual variability in the concentrations of northern hemispheric tracers observed by *Prinn et al.* [1992] in surface air at Samoa. These shifts, affecting the flow of the river of pollution discussed in the previous section, modulate northern hemispheric influences on surface air at equatorial stations without necessarily being associated with interhemispheric exchange. Indeed, surface observations are not the best indicator for upper tropospheric cross-equatorial transport.

PEM-Tropics B provided the first extensive observations of northern hemispheric tracers in the tropical upper troposphere, where the transport across the equator primarily occurs, over a wide longitudinal domain. If convection were the dominant mechanism for interhemispheric exchange, then we would expect concentrations of northern hemispheric tracers in the upper troposphere to be elevated over the western South Pacific, in the vicinity of the warm pool where convection is most intense. Conversely, transport via the westerly duct would enhance concentrations over the eastern South Pacific around 135°–90°W, where the duct is located (Figure 4). Observed CO concentrations in the upper troposphere (Plate 1c) are clearly higher above the eastern Pacific, although South American sources might contribute to this enhancement. We examined the observed longitudinal gradients in the South Pacific upper troposphere (0°–20°S, 8–12 km altitude) for several other tracers of northern hemispheric air, including HCFC-141b, Halon- 1211, and ethyne, as shown in Figure 5; these gradients are insensitive to the exact latitudinal range selected for averaging. All of these tracers have significantly higher concentrations in the eastern Pacific, implying that the westerly duct does dominate over western Pacific ITCZ convection as a mechanism for interhemispheric exchange.

The model reproduces the observed longitudinal gradient of CO concentrations, as shown in Figure 9, and can be used to better quantify the relative importance of the two mechanisms for interhemispheric exchange.

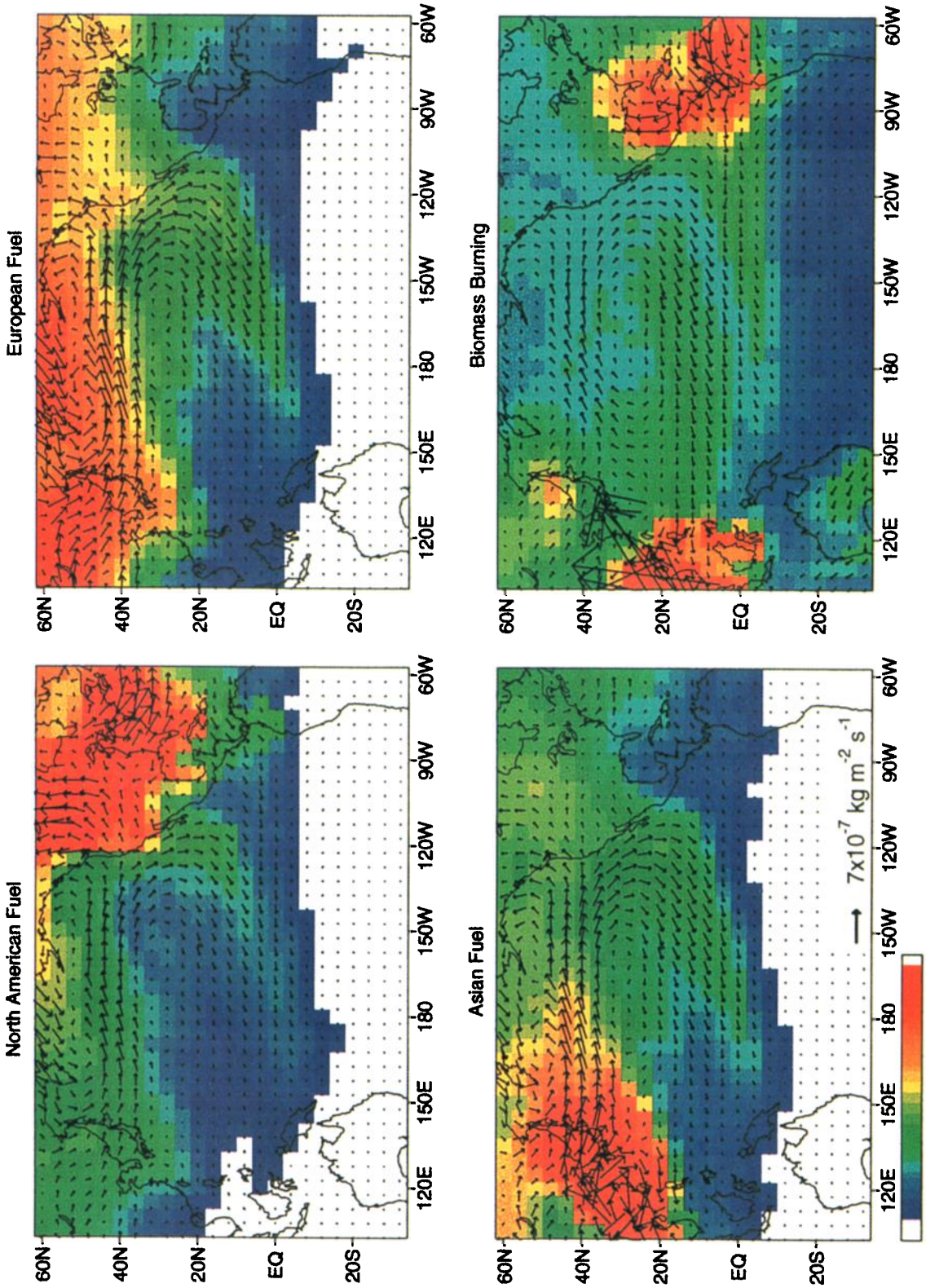

Plate 4. Simulated CO concentrations (ppb) at 0.2–0.6 km altitude for tagged tracers averaged over the PEM-Tropics B time period (March 1 to April 19, 1999). The arrows indicate the tracer horizontal mass fluxes.

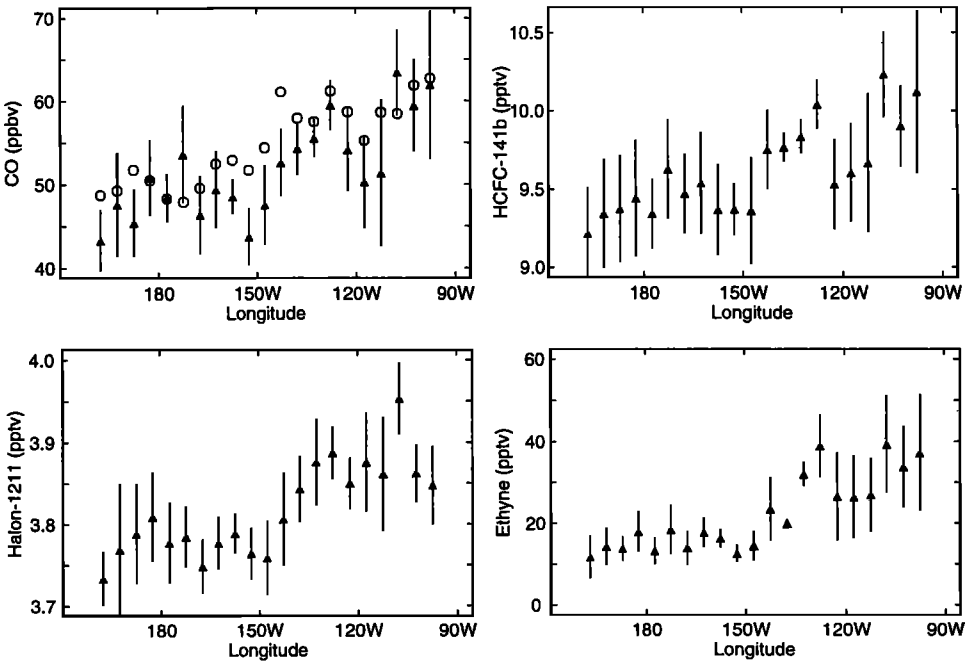

Figure 5. Longitudinal concentration gradients for tracers of northern hemispheric air in the upper troposphere of the southern tropics. The PEM-Tropics B DC-8 observations (black triangles) are averaged over March 1 to April 19, 1999, 8–12 km altitude, 0°–20°S latitude, and 5° longitude bins. Vertical bars indicate standard deviations. The model CO concentrations (open circles) are sampled along the flight tracks and for the flight days, and the results are averaged across nearly the same altitude and latitude ranges as the observations (8–13 km, 2°–22°S).

Figure 6 shows the simulated horizontal fluxes and positive convective tendencies in the upper troposphere (10–13.5 km) for fossil fuel CO emitted from northern hemispheric continents. Regions of strong convection are associated with upper tropospheric divergence. For example, CO is advected away from the warm pool over the western equatorial Pacific to the northeast, northwest, and southwest. From Figure 6 we identify the southwestward transport across the Indian Ocean as one of three major regions of cross-equatorial transport in the upper troposphere. The second, also associated with divergence caused by intense convection over the African continent, is located over the Atlantic Ocean. The third region of southward transport of northern hemispheric tracer is located over the eastern Pacific and is not adjacent to any large convective activity. Instead, this region of northerly flow can be attributed to the westerly duct.

One way to quantify the relative importance of these three transport pathways to the southern hemisphere is to calculate the average rate that northern hemispheric tracers of fossil fuel combustion are transported through a wall situated at 20°S latitude. This latitude is chosen in order to isolate transport that incorporates northern hemispheric tracer into the southern hemispheric circulation. The flux of the sum of northern hemispheric fuel tracers crossing a wall at 20°S is shown in the top panel of Figure 7. As discussed above, three windows of northerly flow are apparent in the upper troposphere above the Indian Ocean, the Atlantic Ocean, and the eastern Pacific Ocean. In addition, two regions of northerly flow of northern hemispheric fossil fuel CO are found in the lower troposphere. The first straddles the date line and represents a combination of flow around the western side of the South Pacific High and transport by the river of pollution across the SPCZ. The second region, situated above South America at 60°W, results when flow around the subtropical West African High coincides with flow around the subtropical South Atlantic High, creating low-level northeasterly winds. Long-range transport of dust from northern Africa to the Amazon via this mechanism was previously observed by *Talbot et al.* [1990] during the Atmospheric Boundary Layer Experiment phase 2B (ABLE 2B) which took place during April-May 1987 [*Harriss et al.*, 1990]. Continued northeasterly flow across South America is impeded by the Andes mountain range, which sends air due south toward a region of convergence located around 20°–25°S and 50°-55°W [*Virji*, 1981; *Figueroa et al.*, 1995]. To assess the relative importance of transport in the lower (below 7.5 km) and upper (7.5–17.5 km) troposphere to interhemispheric exchange, we plot the mean meridional flux of northern hemispheric fossil fuel tracers at 20°S as a function of altitude in Figure 8. The lower troposphere accounts for 25% of the total southward flux in the model. We focus our attention on the upper troposphere for the rest of this analysis.

The bottom panel of Figure 7 shows the meridional flux at 20°S and 7.5–17.5 km altitude as a function of

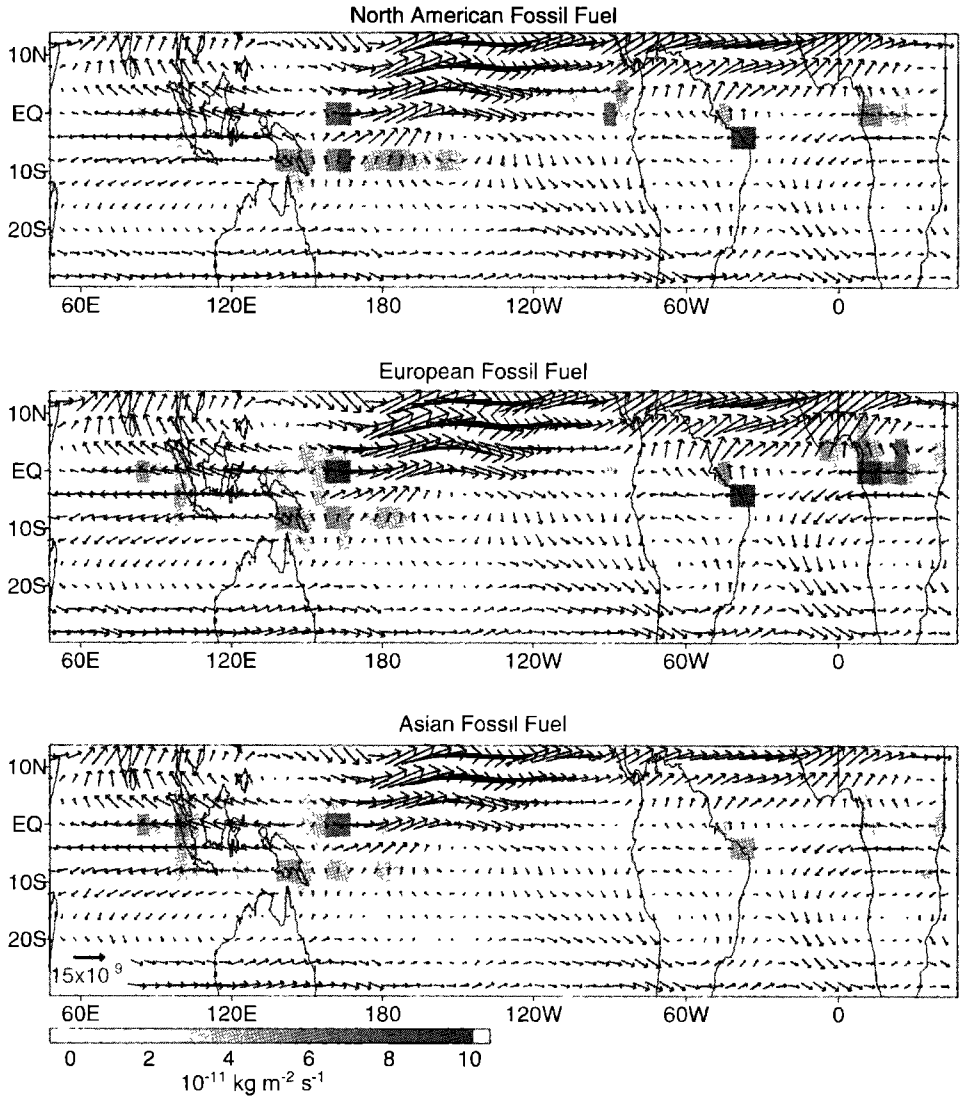

Figure 6. Simulated transport fluxes (kg m^{-2} s^{-1}) of tagged fuel CO from North America, Europe, and Asia at 10–13.5 km altitude. Shading indicates regions with large positive convective tendencies as diagnosed by increases in the 10-13.5 km column of CO (kg m^{-2} s^{-1}) due to convection.

longitude, and separates the contributions from North America, Europe, and Asia. The three pathways identified previously contribute essentially all of the northern hemispheric fossil fuel CO transported southward in the upper troposphere at 20°S. The longitudinal extent of each upper tropospheric window of southward transport is determined by where the mean southward flux is at least 0.3×10^{-9} kg m^{-2} s^{-1}, as indicated by the horizontal line in Figure 7 (bottom panel), and the corresponding flow rates for each region are summarized in Table 3. The westerly duct over the eastern Pacific accounts for 40% of the total northern hemispheric fuel carried southward in the upper troposphere, with comparable contributions from each continent. Despite originating from farthest north, European fuel sources makes the largest contribution of the three continents to interhemispheric exchange of CO, consistent with the wintertime accumulation of a large European CO inventory at high northern latitudes, as discussed in section 4. One would expect the European contribution to interhemispheric exchange of CO and other photochemically destroyed species to be at its seasonal maximum during spring.

7. Summary

We have used a 3-D global chemical transport model driven by assimilated meteorology for the PEM-Tropics B period (March-April 1999) to show how anthropogenic pollution from different source regions in the northern midlatitudes is transported to the North Pacific and from there to equatorial latitudes and to the South Pacific. Our analysis focused on CO, a tracer of incomplete combustion with a sufficient lifetime (months) to enable global-scale transport. The PEM-Tropics B aircraft observations show a strong latitudinal gradient from the

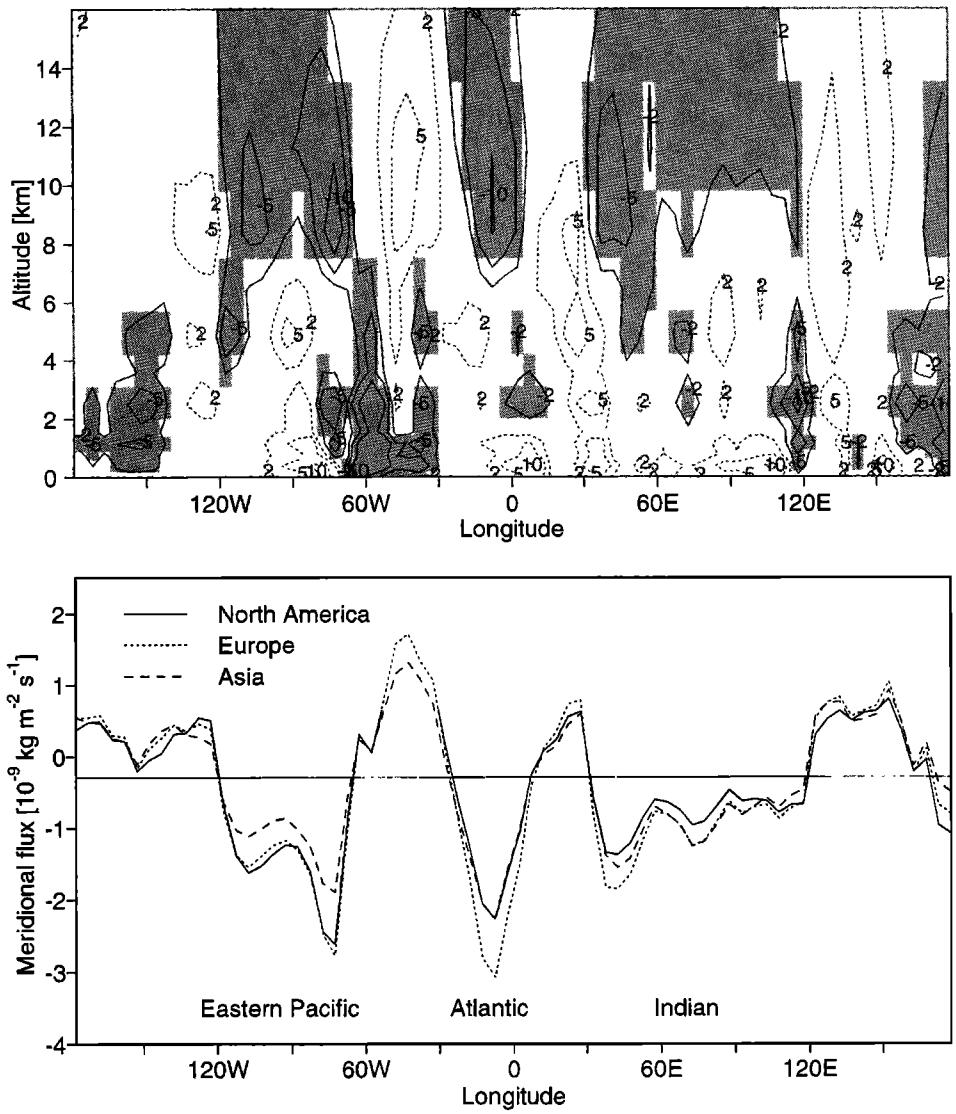

Figure 7. (top) Mean simulated meridional flux (in kg m^{-2} s^{-1}) of CO from northern hemispheric fuel sources (fossil fuel from North America, Europe, and Asia) through a wall at 20°S. Values are averaged for the PEM-Tropics B period (March 1 to April 19, 1999). Negative numbers and shaded regions indicate southward transport. (bottom) The average meridional flux across 20°S in the upper troposphere (7.5 to 17.5 km altitude) simulated for each northern hemispheric source region as a function of longitude.

North to the South Pacific, as would be expected for that season. Concentrations over the equatorial Pacific decrease from west to east in the boundary layer; this longitudinal gradient is reversed in the upper troposphere. Concentrations over the North Pacific decrease with altitude, and the reverse vertical gradient is observed over the South Pacific. The model reproduces the observed concentrations and gradients with only minor discrepancies.

Linear decomposition of CO was conducted in the model to quantify the contributions from different source regions to the overall concentrations of CO over the Pacific during PEM-Tropics B. Asian and European fuel emissions made dominant and comparable anthropogenic contributions to the tropospheric CO burden in the North Pacific region sampled during the campaign (10°–35°N). European emissions were actually more important than Asian emissions as a source of CO over the Pacific north of 35°N. The relatively large European contribution reflects the accumulation of European CO at high northern latitudes during the winter months when photochemical loss of CO is inoperative. The spring timing of PEM-Tropics B probably corresponded to the seasonal maximum of European influence over the North Pacific. North American fuel combustion sources made little contribution to CO anywhere over the Pacific. Biomass burning in Southeast Asia, which is at its seasonal maximum during February-April and was particularly intense in 1999, accounted for 20% of CO over the northeastern Pacific region sampled in

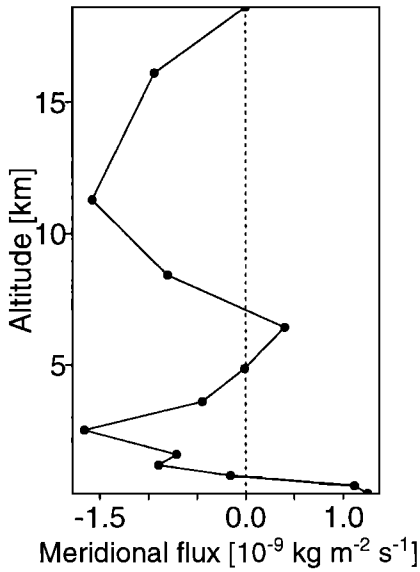

Figure 8. Vertical distribution of the simulated meridional flux (kg m^{-2} s^{-1}) of CO from northern hemispheric fuel sources (fossil fuel from North America, Europe, and Asia) at 20°S. Values are averaged for the PEM-Tropics B period (March 1 to April 19, 1999) and across all longitudes. Negative values indicate southward transport.

PEM-Tropics B and was particularly important in the free troposphere.

A prominent feature of the PEM-Tropics B observations was a river of pollution extending across the equatorial Pacific in which tracers of northern mid-latitude urban and industrial pollution were elevated in the boundary layer from the California coast southwestward to Fiji in the southern hemisphere. The model reproduces the observed CO enhancement in the river of pollution and attributes the enhancement to fuel combustion at northern midlatitudes. Europe and Asia made comparable contributions to this enhancement, while the contribution from North America was much smaller. The river of pollution was fed by southward transport of Eurasian emissions around the Pacific High and into the northern trade winds. Biomass burning was a relatively minor contributor to the boundary layer CO budget in general and to the river of pollution in particular; export of biomass burning effluents from Southeast Asia to the Pacific takes place mainly in the free troposphere at subtropical latitudes where the lifetime of CO is relatively short. It appears that chemical aging during subsidence of air masses near the Pacific High limits the extent to which biomass burning CO contributes to boundary layer concentrations. Biomass burning emissions from Central America and northern South America, which are exported to the Pacific in the northern trade winds, were relatively low during 1999 and made only a minor contribution.

Observations from PEM-Tropics B provided an extensive survey of upper tropospheric composition in both the northern and the southern tropics over a broad range of longitudes. We used these data together with our model to identify mechanisms for interhemispheric exchange. We found that transport through the westerly duct of the eastern Pacific upper troposphere is a major contributor to global interhemispheric exchange, accounting for 40% of transport in the upper troposphere to the southern hemisphere of northern hemispheric fossil fuel CO during the PEM-Tropics B period. The effect of this mechanism is apparent in an enhancement of northern hemispheric pollution tracers in the equatorial upper troposphere of the southeastern Pacific as compared to the southwestern Pacific, both in the observations and in the model. Propagation of Rossby waves through the westerly duct has been shown previously to be the most effective during boreal winter and La Nina conditions. It thus appears that PEM-Tropics B occurred during conditions for maximum interhemispheric transport of trace gases by this mechanism.

Acknowledgments. This work was supported by the NASA Global Trophospheric Chemistry Program. Amanda Staudt was supported by a National Science Foundation Graduate Fellowship. We are grateful to Isabelle Bey and Arlene Fiore for helpful discussions, and to Andrew Fusco and Brendan Field for conducting model runs to obtain initial conditions.

Table 3. Southward Mass Transport of CO Through Windows at 20°S and 8–17 km Altitude[a]

	North American Fossil Fuel	European Fossil Fuel	Asian Fossil Fuel	Total Northern Hemisphere Fossil Fuel
Indian Ocean (35°E–120°E)	46	64	64	174
Atlantic Ocean (20°W–5°E)	35	52	37	124
Eastern Pacific Ocean (120°W–65°W)	80	80	54	214
Total	161	196	155	

[a]Values are model averages for March 1 to April 19, 1999. Units are in kg s^{-1}.

References

Andreae, M.O., and P. Merlet, Emission of trace gases and trace gases and aerosols from biomass burning, *Global Biogeochemical Cycles*, in press, 2001.

Arkin, P. A., The relationship between interannual variability in the 200 mb tropical wind field and the southern oscillation, *Mon. Weather Rev., 110*, 1393–1404, 1982.

Arkin, P. A., and P. J. Webster, Annual and interannual variability of tropical-extratropical interaction: An empirical study, *Mon. Weather Rev., 113*, 1510–1523, 1985.

Balkanski, Y.J., D.J. Jacob, R. Arimoto, and M.A. Kritz, Long-range transport of ^{222}Rn over the North Pacific Ocean: Implications for continental influence, *J. Atmos. Chem., 14*, 353-374, 1992.

Blake, N.J., D. R. Blake, T.-Y. Chen, J. E. Collins Jr., G. W. Sachse, B. E. Anderson, and F. S. Rowland, Distribution and seasonality of selected hydrocarbons and halocarbons over the western Pacific basin during PEM-West A and PEM-West B, *J. Geophys. Res., 102*, 28,315–28,331, 1997.

Blake, N.J., et al., Large-scale latitudinal and vertical distributions of NMHCs and selected halocarbons in the troposphere over the Pacific Ocean during the March-April 1999 Pacific Exploratory Mission (PEM-Tropics B), *J. Geophys. Res.*, this issue.

Bowman, K. P., and P. J. Cohen, Interhemispheric exchange by seasonal modulation of the Hadley circulation, *J. Atmos. Sci., 54*, 2045–2059, 1997.

Christensen, J. H., The Danish Eulerian hemispheric model — A three-dimensional air pollution model used for the Arctic, *Atmos. Environ., 31*, 4169-4191, 1997.

Environmental Protection Agency (EPA), National air pollutant emission trends, 1990–1996, *Rep. EPS-454/R-97-011*, Research Triangle Park, N.C., 1997.

European Monitoring and Evaluation Programme (EMEP), Transboundary air pollution in Europe, part 1, Emissions, dispersion and trends of acidifying and eutrophying agents, *EMEP/MSC-W Rep. 1/97*, Norw. Meteorol. Inst., Oslo, Norway, 1997.

Figueroa, S. N., P. Satyamurty, and P. L. da Silva Dias, Simulations of the summer circulation over the South American region with an eta coordinate model, *J. Atmos. Sci., 52*, 1573–1584, 1995.

Fuelberg, H. E., R. E. Newell, D. J. Westberg, J. C. Maloney, J. R. Hannan, B. C. Martin, M. A. Avery, and Y. Zhu, A meteorological overview of the second Pacific Exploratory Mission in the Tropics, *J. Geophys. Res.*, this issue.

Gairola, R. M., and T. N. Krishnamurti, Rain rates based on SSM/I, OLR and raingauge data sets, *Meteorol. Atmos. Phys., 50*, 165–174, 1992.

Galasyn, J. F., K. L. Tschudy, and B. J. Huebert, Seasonal and diurnal variability of nitric acid vapor and ionic aerosol species in the remote free troposphere at Mauna Loa, Hawaii, *J. Geophys. Res., 92*, 3105–3113, 1987.

Granier, C., G. Petron, J. F. Muller, and G. Brasseur, The impact of natural and anthropogenic hydrocarbons on the tropospheric budget of carbon monoxide, *Atmos. Environ., 34*, 5255–5270, 2000.

Halter, B. C., J. M. Harris, and T. J. Conway, Component signals in the record of atmospheric carbon dioxide concentration at American Samoa, *J. Geophys. Res., 93*, 15,914–15,918, 1988.

Harris, J. M., and S. J. Oltmans, Variations in tropospheric ozone related to transport at American Samoa, *J. Geophys. Res., 102*, 8781–8791, 1997.

Harriss, et al., The Amazon Boundary Layer Experiment: Wet season 1987, *J. Geophys. Res., 95*, 16,721–16,736, 1990.

Hartley, D. E., and R. X. Black, Mechanistic analysis of interhemispheric transport, *Geophys. Res. Lett., 22*, 2945–2948, 1995.

Hoell, J. M., D. D. Davis, S. C. Liu, R. Newell, M. Shipham, H. Akimoto, R. J. McNeal, R. J. Bendura, and J. W. Drewry. The Pacific Exploratory Mission-West Phase A: September-October 1994, *J. Geophys. Res., 101*, 1641–1653, 1996.

Hoell, J. M., D. D. Davis, S. C. Liu, R. E. Newell, H. Akimoto, R. J. McNeal, and R. J. Bendura. The Pacific Exploratory Mission-West Phase B: February-March 1994, *J. Geophys. Res., 102*, 28,223–28,240, 1997.

Hoell, J. M., D. D. Davis, D. J. Jacob, M. O. Rodgers, R. E. Newell, H. E. Fuelberg, R. J. McNeal, J. L. Raper, and R. J. Bendura, Pacific Exploratory Mission in the tropical Pacific: PEM-Tropics A, August-September 1996, *J. Geophys. Res., 104*, 5567–5583, 1999.

Holloway, T., H. Levy II, and P. Kasibhatla, Global distribution of carbon monoxide, *J. Geophys. Res., 105*, 12,123–12,147, 2000.

Horowitz, L. W., J. Y. Liang, G. M. Gardner, D. J. Jacob, Export of reactive nitrogen from North America during summertime, *J. Geophys. Res., 103*, 13,435–13,450, 1998.

Hsu, N. C., J. R. Herman, P. K. Bhartia, C. J. Seftor, O. Torres, A. M. Thompson, J. F. Gleason, T. F. Eck, and B. N. Holben. Detection of biomass burning smoke from TOMS measurements, *Geophys. Res. Lett., 23*, 745–748, 1996.

Huntrieser, H., H. Schlager, C. Feigl, and H. Holler, Transport and production of NO_x in electrified thunderstorms: Survey of previous studies and new observations at midlatitudes, *J. Geophys. Res., 103*, 28,247–28,264, 1998.

Jacob, D. J., M. J. Prather, S. C. Wofsy, and M. B. McElroy, Atmospheric distribution of ^{85}Kr simulated with a general circulation model, *J. Geophys. Res., 92*, 6614–6626, 1987.

Jacob, D. J., J. A. Logan, and P. P. Murti, Effect of rising Asian emissions on surface ozone in the United States, *Geophys. Res. Lett., 26*, 2175–2178, 1999.

Jacobson, M. Z., and R. P. Turco, SMVGEAR: A sparse-matrix, vectorized gear code for atmospheric models, *Atmos. Environ., 28*, 273–284, 1994.

Jaffe, D., A. Mahura, J. Kelley, J. Atkins, P. C. Novelli, and J. Merril. Transport of Asian air pollution to North America, *Geophys. Res. Lett., 26*, 711–714, 1999.

Kanakidou, M., H. B. Singh, K. M. Valentin, and P. J. Crutzen, A two-dimensional study of ethane and propane oxidation in the free troposphere, *J. Geophys. Res., 96*, 15,395–15,413, 1991.

Kanakidou, M., F. J. Dentener, P. J. Crutzen, A global three-dimensional study of the fate of HCFCs and HFC-134a in the troposphere, *J. Geophys. Res., 100*, 18,781–18,801, 1995.

Kidson, J. W., D. G. Vincent, and R. E. Newell, Observed studies of the general circulation of the Tropics: Long term mean values, *Q. J. R. Meteorol. Soc., 95*, 258–287, 1969.

Krishnamurti, T. N., S. Low-Nam, and T. Pasch, Cumulus parameterization and rainfall rates II, *Mon. Weather Rev., 111*, 815–828, 1983.

Krishnamurti, T. N., H. E. Fuelberg, M. C. Sinha, D. Oosterhof, E. L. Bensman, and V. B. Kumar, The meteorological environment of the tropospheric ozone maximum over the tropical South Atlantic, *J. Geophys. Res., 98*, 10,621–10,641, 1993.

Krishnamurti, T. N., M. C. Sinha, M. Kanamitsu, D. Oosterhof, H. Fuelberg, R. Chatfield, D. J. Jacob, and J. A. Logan, Passive tracer transport relevant to the TRACE-A experiment, *J. Geophys. Res., 101*, 23,889–23,907, 1996.

Logan, J. A., I. Megretsakaia, D. Blake, G. Sachse, B. Martin, and H. Fuelberg, Signatures of northern hemispheric

air in the southern hemisphere (and vice-versa) in PEM-Tropics B (abstract), *Eos Trans. AGU, 81*(19), Spring Meet. Suppl., Abstract no. A31E-06, 2000.

Marland, G., T. A. Boden, R. J. Andres, A. L. Brenkert, and C. A. Johnston, Global, regional, and national fossil fuel CO_2 emissions, in *Trends: A Compendium of Data on Global Change Carbon Dioxide Information Analysis Center*, Oak Ridge Nat. Lab., U.S. Dep. of Energy, Oak Ridge, Tenn., 1999.

Merrill, J. T., Atmospheric long-range transport to the Pacific Ocean, in *Chemical Oceanography*, vol. 10, edited by R. A. Duce, J. P. Riley, and R. Chester, pp. 15–50, Academic, San Diego, Calif., 1989.

Mickley, L. J., P. P. Murti, D. J. Jacob, J. A. Logan, D. Rind, and D. Koch, Radiative forcing from tropospheric ozone calculated with a unified chemistry-climate model, *J. Geophys. Res., 104*, 30,153–30,172, 1999.

Moxim, W. J., Simulated transport of NO_y to Hawaii during August: A synoptic study, *J. Geophys. Res., 95*, 5717–5729, 1990.

Newell, R. E., G. J. Boer Jr., and J. W. Kidson, An estimate of the interhemispheric transfer of carbon monoxide from tropical general circulation data, *Tellus, 26*, 103–107, 1974.

Newell, R. E., Y. Zhu, E. V. Browell, W. G. Read, and J. W. Waters, Walker circulation and tropical upper tropospheric water vapor, *J. Geophys. Res., 101*, 1961–1974, 1996.

Novelli, P. C., K. A. Masarie, and P. M. Lang, Distributions and recent changes of carbon monoxide in the lower troposphere, *J. Geophys. Res., 103*, 19,015–19,033, 1998.

Pak, B. C., R. L. Langenfelds, R. J. Francey, L. P. Steele, and I. Simmonds, A climatology of trace gases from the Cape Grim overflights, 1992–1995, in *Baseline Atmospheric Program (Australia) 1994–95*, edited by R. G. Francey, A. L. Dick, and N. Derek, pp. 41–52, Bur. of Meteorol. and CSIRO Div. of Atmos. Res., Melbourne, Victorial, Australia, 1996.

Pickering, K.E., Y. Wang, W.-K. Tao, C. Price, and J.-F. Muller, Vertical distributions of lightning NO_x for use in regional and global chemical transport models, *J. Geophys. Res., 103*, 31,203–31,216, 1998.

Pougatchev, N. S., G. W. Sachse, H. E. Fuelberg, C. P. Rinsland, R. B. Chatfield, V. S. Conners, N. B. Jones, J. Notholt, P. C. Novelli, and H. G. Reicle Jr., Pacific Exploratory Mission-Tropics carbon monoxide measurements in historical context, *J. Geophys. Res., 104*, 26,195–26,207, 1999.

Prather, M. J., Numerical advection by conservation of second-order moments, *J. Geophys. Res., 91*, 6671–6781, 1986.

Prather, M. J., M. McElroy, S. Wofsy, G. Russell, and D. Rind, Chemistry of the global troposphere: Fluorocarbons as tracers of air motion, *J. Geophys. Res., 92*, 6579–6613, 1987.

Price, C., and D. Rind, A simple lightning parameterization for calculating global lightning distributions, *J. Geophys. Res., 97*, 9919–9933, 1992.

Prinn, R., et al., Global average concentration and trend for hydroxyl radicals deduced from ALE/GAGE trichloroethane (methylchloroform) data for 1978–1990, *J. Geophys. Res., 97*, 2445–2461, 1992.

Prinn, R. G., R. F. Weiss, B. R. Miller, J. Huang, F. N. Alyea, D. M. Cunnold, P. J. Fraser, D. E. Hartley, and P. G. Simmonds, Atmospheric trends and lifetime of CH_3CCl_3 and global OH concentrations, *Science, 269*, 187–192, 1995.

Raatz, W. E., An anticyclonic point of view on low-level tropospheric long-range transport, *Atmos. Environ., 23*, 2501–2504, 1989.

Raper, J. L., M. M. Kleb, D. J. Jacob, D. D. Davis, R. E. Newell, H. E., Fuelberg, R. J. Bendura, J. M. Hoell, and R. J. McNeal, Pacific Exploratory Mission in the tropical Pacific: PEM-Tropics B, March-April 1999, *J. Geophys. Res.*, this issue.

Sachse, G. W., G. F. Hill, L. O. Wade, and M. G. Perry, Fast-response, high-precision carbon monoxide sensor using a tunable diode laser absorption technique, *J. Geophys. Res., 92*, 2071–2081, 1987.

Sachse, G. W., J. E. Collins Jr., G. F. Hill, L. O. Wade, L. G. Burney, and J. A. Ritter, Airborne tunable diode laser sensor for high precision concentration and flux measurements of carbon monoxide and methane, *Proc. SPIE Int. Soc. Opt. Eng., 1443*, 145–156, 1991.

Schultz, M. G., et al., On the origin of tropospheric ozone and NO_x over the tropical south Pacific, *J. Geophys. Res., 104*, 5829–5844, 1999.

Spivakovsky, C. M., et al., Three-dimensional climatological distribution of tropospheric OH: Update and evaluation, *J. Geophys. Res., 105*, 8931–8980, 2000.

Talbot, R. W., M. O. Andreae, H. Berresheim, P. Artaxo, M. Garstang, R. C. Harriss, K. M. Beecher, and S. M. Liu, Aerosol chemistry during the wet season in central Amazonia: The influence of long-range transport, *J. Geophys. Res., 95*, 16,955–16,969, 1990.

Thompson, A.M., The oxidizing capacity of the Earth's atmosphere: Probable past and future changes, *Science, 256*, 1157–1165, 1992.

Tomas, R. W., and P. J. Webster, Horizontal and vertical structure of cross-equatorial wave propagation, *J. Atmos. Sci., 51*, 1417–1430, 1994.

Virji, H., A preliminary study of summertime tropospheric circulation patterns over South America estimated from cloud wind, *Mon. Weather Rev., 109*, 599–610, 1981.

Wang, Y., D. J. Jacob, and J. A. Logan, Global simulation of tropospheric O_3-NO_x-hydrocarbon chemistry, 1, Model formulation, *J. Geophys. Res., 103*, 10,713–10,726, 1998a.

Wang, Y., J. A. Logan, and D. J. Jacob, Global simulation of tropospheric O_3-NO_x-hydrocarbon chemistry, 2, Model evaluation and global ozone budget, *J. Geophys. Res., 103*, 10,727–10,756, 1998b.

Wang, Y., et al., Factors controlling tropospheric O_3, OH, NO_x, and SO_2 over the tropical Pacific during PEM-Tropics B, *J. Geophys. Res.*, this issue.

Webster, P., and J. Holton, Cross-equatorial response to middle-latitude forcing in a zonally varying basic state, *J. Atmos. Sci., 39*, 722–733, 1982.

Wild, O., Z. Xin, and M. J. Prather, Fast-J: Accurate simulation of in- and below-cloud photolysis in Global Chemical Models, *J. Atmos. Chem., 37*, 245–282, 2000.

Yienger, J. J., M. Galanter, T. A. Holloway, M. J. Phadnis, S. K. Guttikunda, G. R. Carmichael, W. J. Moxim, and H. Levy II, The episodic nature of air pollution transport from Asia to North America, *J. Geophys. Res., 105*, 26,931–26,945, 2000.

D. Bachiochi and T. N. Krishnamurti Department of Meteorology, Florida State University, Tallahasse, FL 32306

D. J. Jacob, J. A. Logan, and A. C. Staudt, Division of Engineering and Applied Sciences and Department of Earth and Planetary Sciences, Harvard University, 29 Oxford St., Cambridge MA 02138. (acs@io.harvard.edu)

G. W. Sachse NASA Langley Research Center, Hampton, VA 23681

(Received October 13, 2000; revised January 19, 2001; accepted January 22, 2001.)